Embedding a Water Vapor Radiometer in a Deep Space Network Ka-Band Beam-Waveguide Receiver: A Feasibility and Performance Evaluation

A. B. Tanner[1] and J. E. Fernandez[2]

This article evaluates the performance of a radiometer concept that would use existing 32-GHz (Ka-band) Deep Space Network (DSN) cryogenic receivers to measure tropospheric water vapor and associated radio path-delay fluctuations on 100-s time scales. The atmospheric signal would be derived from noise temperature fluctuations detected at the output of the cryogenic high-electron-mobility transistor (HEMT) low-noise amplifier (LNA) using a power meter in an unused passband of the receiver. Three errors are examined: (1) retrieval, (2) instrument stability, and (3) antenna side-lobe contamination. Retrieval errors estimated from recent Cassini tropospheric calibration data indicate that, in principle, a single-frequency 32-GHz measurement could just meet Gravitational Wave Experiment 100-s Allan standard deviation (ASD) requirements of 4.5×10^{-15} s/s on most cloud-free days at Goldstone. However, new gain stability measurements of the DSN HEMT LNAs are reported that translate to a 100-s ASD of 8.7×10^{-15} s/s. Antenna side lobes contribute up to 7.5×10^{-15} s/s of additional error for elevation angles above 45 deg and up to 22.5×10^{-15} s/s for an elevation of 20 deg, based on data collected last year at DSS 13. The root-sum-square (rss) of these and other errors yields a net error of about 10×10^{-15} s/s to 27×10^{-15} s/s of ASD at 100 s. These errors are comparable to the uncalibrated atmosphere at Goldstone while viewing zenith on dry winter days, in which case the radiometric data would be of limited value. On more humid days, the retrieved path delay may be helpful. For example, from the Cassini passes examined as part of this study, 6 of 11 passes exceeded 30×10^{-15} s/s in the uncalibrated line-of-sight ASD at 100 s.

I. Introduction

Water vapor in the Earth's troposphere adds an unwanted variable delay to radio signals that pass through the atmosphere. With advances in frequency standards and the move to 32-GHz (Ka-band) space-

[1] Microwave and Lidar Technology Section.

[2] Communications Ground Systems Section.

The research described in this publication was carried out by the Jet Propulsion Laboratory, California Institute of Technology, under a contract with the National Aeronautics and Space Administration.

craft communications, this "wet" path delay is increasingly seen as a limiting error for precise spacecraft tracking and for very long baseline interferometry (VLBI). Water vapor radiometers (WVRs) provide a means of correcting the wet path-delay error by observing water vapor emissions near an absorption line at 22 GHz. The latest example of such a system is the tropospheric calibration (tropo-cal) system, which was recently deployed at DSS 25 to support the Cassini Gravitational Wave Experiment (GWE). The tropo-cal system includes a comprehensive set of instrumentation, including two advanced water vapor radiometers (AWVRs) and microwave temperature profilers. These radiometers were designed to meet very stringent requirements for the path-delay measurement on long time scales of 1,000 to 10,000 s [1]. On shorter time scales of 100 s or less, however, the performance of this system degrades, due in part to the fact that the AWVR antennas are offset from the DSS-25 antenna by about 40 m [2]. This article investigates a very low cost system that would derive a radiometric measurement from operational cryogenic 32-GHz receivers in the DSS-25 optics to improve upon the path-delay performance at short time scales. Such an embedded system would have the inherent advantage of sampling precisely the same volume of atmosphere that is responsible for the radio path delay. The embedded system would also have the advantage of a cryogenically cooled front end, which helps the performance at short time scales.

Technical problems associated with an embedded radiometer system include calibration difficulties and incompatible observation frequencies. Ideally, an embedded WVR would operate at several frequencies from 22 GHz to 32 GHz in order to separate the effects of clouds and water vapor, among other factors. Yet the existing Ka-band low-noise amplifier (LNA) at DSS 25 only passes 31.5 to 32.5 GHz. Obtaining all the desired bands would require costly modifications to the communication system, which must already contend with a complex mix of 8 GHz (X-band), Ka-band, uplink, and downlink requirements. The calibration of an embedded system would also be difficult given the scattered losses of DSN antennas and the fact that a chopped reference (Dicke switch) can't be readily introduced without interfering with the communication function. Many of these problems are reduced by considering only the clear-sky (i.e., cloud-free) path-delay fluctuations on 100-s time scales. To minimize the costs, this article will focus on a system that would use only the available observation band at 32 GHz. Such a system would be very low in cost as it would require only the addition of a power meter to monitor the noise temperature at the output of the existing cryogenic 32-GHz high-electron-mobility transistor (HEMT) LNA. Risk to the operational receiver would be low.

The path-delay performance of a single-frequency 32-GHz embedded water vapor radiometer system will be examined in three parts: (1) retrieval errors—meaning errors associated with the non-unique mapping of brightness temperature at 32 GHz to radio path delay; (2) instrument stability—which considers the noise equivalent delta-T (NEDT) of the brightness-temperature measurement given the gain stability and noise temperature of the HEMT LNA on 100-s time scales; and (3) antenna side-lobe contamination. Retrieval errors and instrument stability errors will be discussed in Sections II and III, respectively. In Section IV, antenna side-lobe effects are discussed. Estimated combined errors from all sources are summarized in Section V.

II. Retrieval Errors of a Single-Frequency 32-GHz Radiometer

Uncertainties in the vertical distribution and temperature of water vapor in the troposphere lead to uncertainties in the path delay derived from a brightness-temperature measurement. These errors have often been assessed by comparing brightness temperatures and path delays computed with radio absorption and refraction models from archives of radiosonde profile data at a given location. With a statistically sufficient set of radiosondes, the standard deviation about a linear regression of these data provides a measure of retrieval error for the total path delay. Yet radiosonde data are typically available only twice a day. This article is concerned with the ability to estimate *changes* in the path delay with changes in the brightness temperature on 100-s time scales, and it is necessary to obtain atmospheric measurements at a comparable rate. The following analysis will derive such a data set from path-delay measurements made by the AWVRs during recent Cassini passes. The AWVR includes an observation

band near 32 GHz—at 31.4 GHz—along with channels at 22.2 and 23.8 GHz. The "true" path delay will be estimated with a three-frequency retrieval algorithm and then compared with the delay obtained with a single-frequency retrieval algorithm. The underlying assumption is that the three-frequency algorithm is superior to the single-frequency one. Radiosonde data will first be used to derive the retrieval formulas and to test this assumption.

Path-delay retrieval formulas and retrieval errors were computed by multi-variable linear regression from an existing archive of radiosonde-based path delays and brightness temperatures. The archive was originally developed for Cassini tropo-cal from over 3 years of radiosonde launches at Desert Rock, Nevada, where atmospheric conditions are comparable to Goldstone. A brief summary of the linear regressions is given in Table 1 along with some statistics of the archive. All of the statistics in Table 1 apply to clear-sky conditions—which prevailed in 90 percent of all radiosondes. The remaining 10 percent of the archive contained significant clouds, and these were included only to compute the all-weather retrieval formula of Table 1.

The first three retrieval errors of Table 1 compare the "true" path delay, P_d, of the archive with the respective retrievals. It is interesting to note that the coefficients of the three-frequency all-weather formula differ greatly from the three-frequency clear-weather formula. The all-weather formula uses the 31.4-GHz channel to negate the corrupting effects of the clouds, as is evident with the negative coefficient of the 31.4-GHz channel. The all-weather formula also ignores the 22.2-GHz brightness temperature, T_{b22}, favoring instead 23.8 GHz as the primary channel for sensing path delay. The three-frequency clear-weather formula, on the other hand, makes use of all three channels to minimize errors associated with the uncertain vertical profile of temperature and vapor in the troposphere.

Table 1. Brief analysis of retrieval performance associated with various combinations of WVR frequencies. Path delays and brightness temperatures were computed from physical models using water vapor and temperature profiles provided by radiosondes.

Desert Rock radiosonde archive statistics	
Number of cloud-free radiosondes:	1833
Brightness temperature range at 31.4 GHz (T_{b31}):	9.77 K ~ 31.49 K
Brightness temperature range at 22.2 GHz (T_{b22}):	9.65 K ~ 101.70 K
Brightness temperature range at 23.8 GHz (T_{b23}):	9.17 K ~ 76.68 K
Path delay (P_d) range:	1.26 K ~ 31.06 cm
Average P_d:	7.78 cm
Standard deviation of P_d:	3.83 cm

Path delay retrieval formulas (P_d in cm, T_{bff} in K at frequency ff in GHz)	
3-frequency all-weather:	$P_d = 0.31 \quad 0.300 \times T_{b31} + 0.012 \times T_{b22} + 0.482 \times T_{b23}$
3-frequency clear-weather:	$P_d = 6.57 + 0.707 \times T_{b31} + 0.259 \times T_{b22} \quad 0.144 \times T_{b23}$
31-GHz single-frequency:	$P_d = 11.09 + 1.34 \times T_{b31}$

Retrieval performance for clear conditions (rms P_d error)	
True P_d versus 3-frequency all-weather retrieval:	0.35 cm
True P_d versus 3-frequency clear-weather retrieval:	0.13 cm
True P_d versus 31-GHz single-frequency retrieval:	0.41 cm
31-GHz single-frequency versus 3-frequency clear-weather retrievals:	0.42 cm

Figures 1 and 2 show the detailed distribution of the same retrieval errors versus path delay for the three-frequency clear-weather and the 31-GHz single-frequency formulas, respectively.

Table 1, as well as Figs. 1 and 2, clearly demonstrates that the three-frequency clear-weather algorithm yields less error than does the 32-GHz retrieval, as expected. Yet the 32-GHz retrieval errors are not bad; the standard deviation of these errors is about 1/10th of the archive path-delay variability. Indeed, such performance is comparable to the all-weather algorithm error in Table 1.

The last entry in Table 1 gives the standard deviation of the path-delay retrieval difference between the three-frequency clear-weather algorithm and the single-frequency 32-GHz algorithm. Figure 3 shows the scatter plot of the same data. Note that the differences in Fig. 3 and the standard deviation of Table 1 are very close to the 32-GHz retrieval errors. This comparison is useful as it shows that 32-GHz retrieval errors can be estimated directly from three-frequency WVR data. This relation will be used below to estimate 31-GHz retrieval errors in terms of Allan standard deviation from AWVR data collected at Goldstone.

Recent Cassini tracking data from the AWVRs were used to evaluate 31-GHz retrievals by comparison with the three-frequency clear-weather retrievals. Figures 4 and 5 give an example of the detailed brightness-temperature time series and the associated Allan standard deviations (ASDs), respectively, for

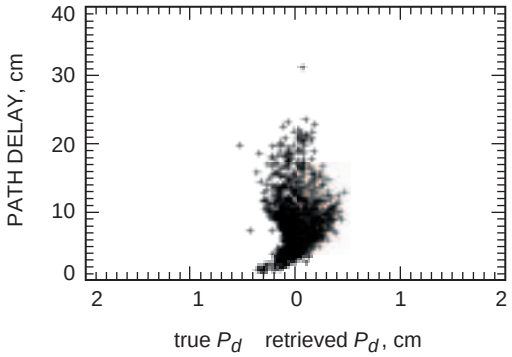

Fig. 1. Errors associated with the three-frequency clear-weather path-delay retrieval of Table 1. Each point represents a single radiosonde.

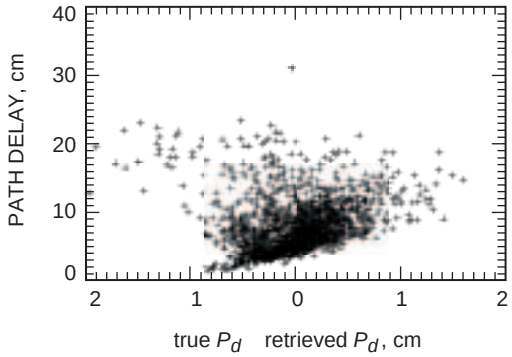

Fig. 2. Errors associated with the single-frequency retrieval of Table 1.

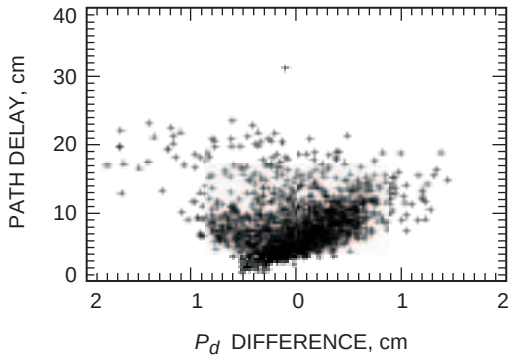

Fig. 3. Difference of the three-frequency clear-weather retrieval and the single-frequency 31-GHz retrieval. By comparison with Figs. 1 and 2, the errors here are clearly dominated by the 31-GHz retrieval errors.

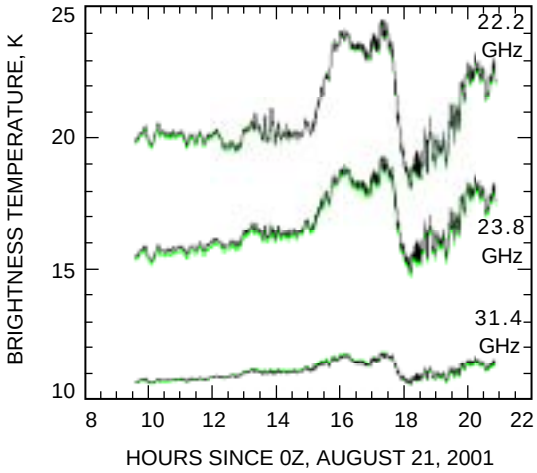

Fig. 4. Examples of T_b's used for ASD analysis in Table 2. An overlay of the AWVR is plotted in green. The 40-s boxcar averages have been applied to this plot. The ASD calculations were based on a finer time grid of 2 s.

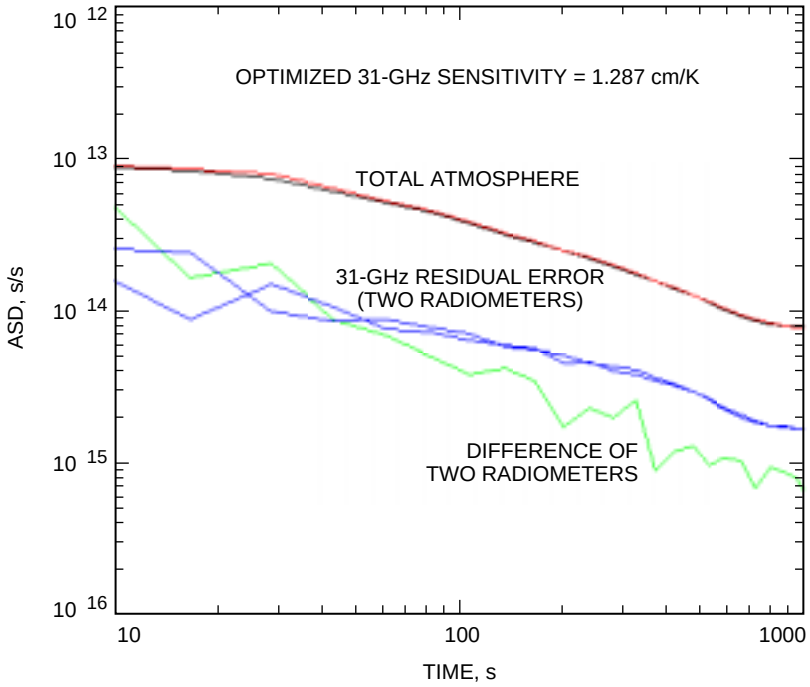

Fig. 5. Example of ASDs computed from the two AWVRs (serial numbers A1 and A2) while following a Cassini track on August 21, 2001, from DSS 25.

one of the passes. All brightness temperatures were mapped to zenith-equivalent brightness temperatures prior to the path-delay estimations and the ASD calculations. The ASD of the total atmosphere was calculated using the three-frequency and 31-GHz retrievals given in Table 1. The 31-GHz sensitivity of Table 1 was then adjusted from the nominal value of 1.34-cm path delay per K brightness temperature to 1.29 cm/K in order to fit the 31-GHz ASD to that of the three-frequency algorithm. The 31-GHz retrieved path-delay time series were then subtracted from the three-frequency retrievals, and the ASDs of the results were calculated and plotted in Fig. 5. Two such estimates of the 31-GHz retrieval errors were plotted from the two AWVRs.

In Fig. 5, the black and red traces represent the zenith equivalent total atmospheric path delay as measured by the A1 radiometer using the three-frequency clear-sky retrieval coefficients of Table 1 (black) and the single-frequency 31-GHz sensitivity coefficient of 1.287 cm/K (red). The two blue traces represent the differences of the three-frequency and single-frequency retrievals for each radiometer and are representative of the 31-GHz single-frequency retrieval errors. The green trace represents the difference of the two radiometers using the 3-frequency retrieval formula; the radiometers are separated by about 40 m, so these errors should approximate similar errors caused by the offsets between the AWVR and the DSS-25 antenna.

Table 2 summarizes the ASD results from 11 Cassini passes in August of 2001. ASD estimates of the atmosphere and of the three-frequency versus 31.4-GHz residuals are given. The zenith-mapped results refer to the ASD computed from zenith equivalent brightness temperature. The line-of-sight ASDs represent the actual path-delay performance along a line of sight to the spacecraft at elevations between 20 and 80 deg.

It is important to note that radiometric noise has been estimated and subtracted from all of the ASD estimates in Fig. 5 and Table 2. The noise was estimated from the 1-s ASD, and then subtracted in quadrature from the ASDs at all time scales. This process yields an ASD that should be representative of atmosphere alone—especially at time scales of 100 s or more. At 10-s time scales, the ratio of atmospheric variability to radiometric noise is very low, so the noise subtraction is less reliable. In Fig. 5, for example, the errors associated with the noise subtraction are apparent where the two 31-GHz retrieval error estimates—taken from two independent radiometers—disagree significantly at 10 s.

The last column of Table 2 gives 31-GHz retrieval error ASDs as a fraction of the total atmosphere ASDs. It is interesting to compare these ratios to the ratio of standard deviations computed from radiosondes: from Table 1, the 31-GHz error versus atmosphere is 0.11 (=0.42 cm/3.83 cm). This ratio is comparable to most of the entries in Table 2. These data support the idea that retrieval errors tend to scale with the atmospheric statistics at all time scales.

III. Instrument Stability

Tests were performed on a DSN 32-GHz cryogenic HEMT amplifier to determine whether the gain stability of the DSN Ka-band receivers would be sufficient for the water vapor measurement. The tests involved simultaneous input and output power measurements using a continuous wave (CW) source at 32 GHz, two power detectors, and two digital volt meters to measure and record the detector voltages. The observed detector voltage fluctuations were near the resolution threshold of the digital voltmeters, so two tests were performed at two power levels separated by 10 dB to verify that fluctuations in the recorded voltages were due to RF power fluctuations and not noise in the voltmeters. Figures 6 and 7 give the raw detected voltages for both tests. Note that Fig. 7 shows a large common mode drop at approximately 7000 s; this drop matches the room temperature of Fig. 8. The voltages in all cases have been normalized to the initial values given in Figs. 6 and 7. The ratio of normalized output to input voltage is also plotted in Figs. 6 and 7. The output/input ratio of Fig. 7 is evidently insensitive to room temperature.

Table 2. Analysis of recent Cassini WVR observations.

Date	31-GHz sensitivity,[a] cm/K	100-s ASD atmosphere,[b] 10^{-15} s/s	100-s ASD 31-GHz retrieval error,[c] 10^{-15} s/s	Retrieval/ atmosphere[d]
		Zenith mapped		
08/18/2001	1.29	20.6	2.63	0.128
08/20/2001	1.24	20.4	2.36	0.116
08/21/2001	1.29	37.0	6.58	0.178
08/22/2001	1.23	15.5	0.99	0.064
08/23/2001	1.16	21.4	2.34	0.110
08/24/2001	1.27	24.2	3.69	0.153
08/25/2001	1.25	9.2	2.08	0.226
08/26/2001	1.32	17.4	1.78	0.103
08/28/2001	1.32	12.5	3.36	0.269
08/30/2001	1.24	16.0	2.20	0.137
09/01/2001	1.19	29.0	2.56	0.088
		Line of sight: 20- to 80-deg elevation		
08/18/2001	1.32	32.6	4.54	0.139
08/20/2001	1.24	30.9	3.64	0.118
08/21/2001	1.29	51.6	7.36	0.143
08/22/2001	1.25	21.7	3.28	0.151
08/23/2001	1.19	33.5	3.82	0.114
08/24/2001	1.28	36.5	5.50	0.151
08/25/2001	1.33	12.9	3.78	0.294
08/26/2001	1.36	29.4	3.03	0.103
08/28/2001	1.39	19.1	5.12	0.268
08/30/2001	1.26	22.4	3.45	0.154
09/01/2001	1.20	50.7	3.76	0.074

[a] Adjusted to minimize the rms error with respect to the three-frequency algorithm.

[b] Computed with the three-frequency clear-weather algorithm of Table 1.

[c] Estimated from the difference of the three-frequency clear-weather and 31-GHz single-frequency retrievals using the formulas of Table 1.

[d] The 31-GHz retrieval error ASDs as a fraction of the total atmosphere ASDs.

The amplifier gain data of Figs. 6 and 7 were analyzed in terms of a modified definition of Allan standard deviation as follows:

$$\mathrm{ASD}_g(\tau) = \left\langle \frac{1}{2}\left[g(t) - 2g(t+\tau) + g(t+2\tau)\right]^2 \right\rangle^{1/2}$$

where $g(t)$ is the normalized output/input amplifier gain (normalized by dividing by an initial value) versus time, t. This definition differs from the conventional ASD in that $g(t)$ is not proportional to a time delay and there is no division by τ. The ASD_g's of the two amplifier tests are plotted in Fig. 9.

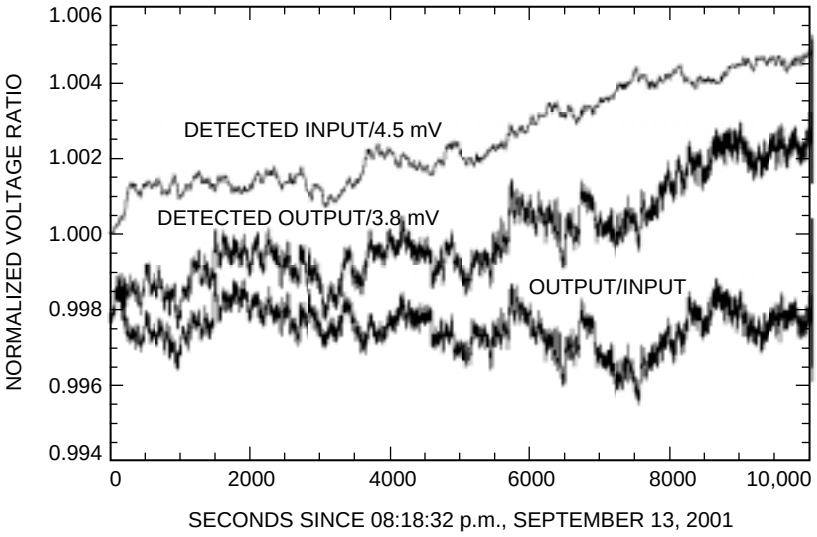

Fig. 6. Raw voltages from HEMT amplifier tests on September 13, 2001.

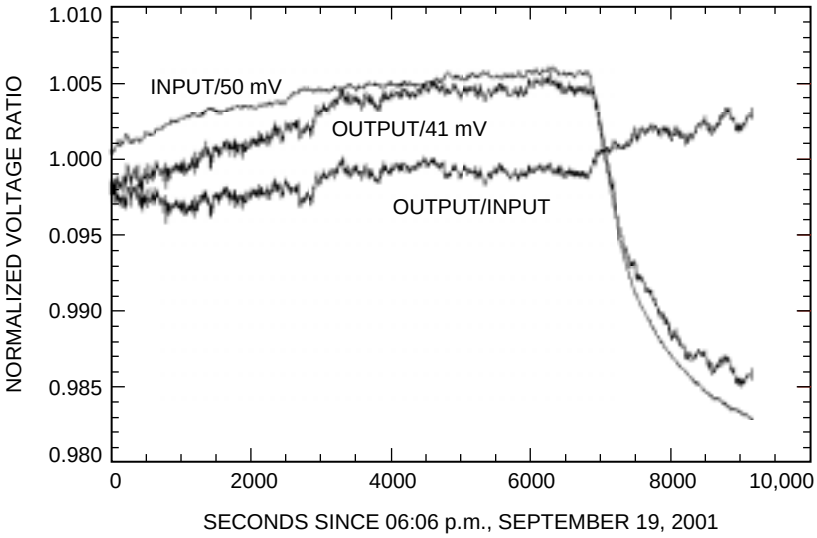

Fig. 7. Data collected September 19, 2001, at a higher signal level and faster data rate of approximately 20 samples/s; 150-sample (or 7.5-s) boxcar averages have been applied.

The two traces agree very well, which indicates that the measurements were of very good quality. The measurement noise of Fig. 9 was computed from data collected at the fast sample rate while the RF source was switched off.

The ASD of Fig. 9 can be readily converted to an ASD in the retrieved path delay by (1) multiplying the gain stability from Fig. 9 by the system noise temperature to obtain a brightness-temperature error in kelvins; (2) scaling the brightness-temperature error to a path-delay error with the 1.34-cm/K sensitivity of Table 1; and then (3) dividing by the speed of light and by τ to obtain the ASD in seconds/second. The receiver noise of the DSN receivers is approximately 30 K—including beam-waveguide losses—and the atmosphere at zenith is approximately 10 K. So, the system noise temperature is about 40 K. Combining these with a gain ASD from Fig. 9 of 0.0005 thus yields a path-delay ASD of 8.7×10^{-15} s/s

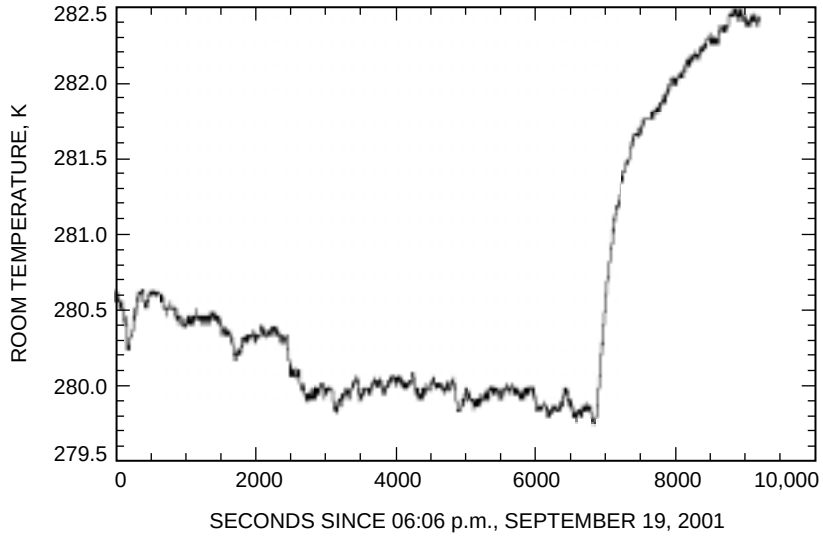

Fig. 8. Room temperatures, K, for the same time scale as in Fig. 7. Correlation with the detected voltage is evident, but the impact on the output/input ratio appears to be negligible.

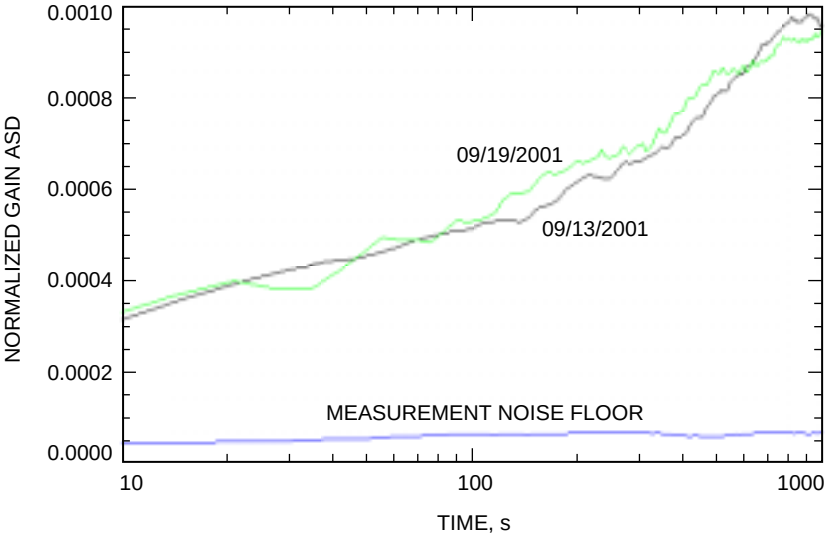

Fig. 9. ASD$_g$ computed from the output/input ratios of Figs. 6 and 7.

at 100 s. At lower elevations, the system noise will increase somewhat: at 20-deg elevation, the atmosphere will present about 30 K to bring the system noise to 60 K and the corresponding 100-s ASD to 13.1×10^{-15} s/s.

The system noise temperature, T_{sys}; bandwidth, B; and the available integration time, τ_I, also set the theoretical thermal noise limit given by the familiar equation

$$\Delta T_N = \frac{T_{sys}}{\sqrt{B\tau_I}}$$

The bandwidth available for an embedded radiometer has not yet been determined, but likely would be near 100 MHz. For an assumed integration time of 10 s and T_{sys} = 40 to 60 K, the above equation

yields about 1.3 mK to 1.9 mK of noise. To scale this noise to an ASD, one multiplies by the path-delay sensitivity of 1.34 cm/K, and then by $\sqrt{3}/c\tau$. At $t = 100$ s, this calculation yields 1.0×10^{-15}-s/s and 1.5×10^{-15}-s/s ASDs at 100 s for 90- and 20-deg elevations, respectively. These noise estimates are compared with other errors in Table 3 in Section V.

IV. Antenna Side-Lobe Contamination

Side lobes of the beam-waveguide antenna are a potentially serious problem for the atmospheric path-delay measurement. At DSS 13, for example, estimated side-lobe losses due to reflector spillover and scattering from support structures have been estimated at about 10 percent [3], which is large for a radiometer. Side lobes that move during an observation between the cold sky and the radiometrically warm terrain surrounding the antenna pedestal are particularly worrisome since the associated antenna noise temperature change might exceed that of the atmosphere.

Last year some tests were conducted at DSS 13 to evaluate the radiometric performance of a beam-waveguide antenna [4]. These tests were conducted with one AWVR located outside and to the south of DSS 13, and the sensor electronics of the second AWVR located at the focal point of the beam-waveguide antenna in the pedestal room. These tests produced measurements of the antenna noise temperature versus antenna position that are directly applicable to the present problem.

Comparisons of the brightness temperatures measured by the embedded and external AWVRs revealed that although the total beam-waveguide losses were quite high—contributing some 6 to 12 K to the antenna noise temperature depending on feedhorn gain and antenna position—the fine structure of these losses versus antenna movement was very low. Upon fitting the measured antenna losses to a three-term Fourier expansion versus azimuth, residual errors for small antenna movements of 0.5 to 4 deg in azimuth were at or below a measurement floor of 0.01 K at elevations of 45 deg or higher. At 20 deg of elevation, the noise temperature fluctuations versus small azimuth motions were about 0.03 K. These errors provide a rough estimate of side-lobe errors encountered on 100- to 1000-s time scales, given a sidereal tracking rate of 0.004 deg/s. These T_B errors have been scaled to the ASD values summarized in the following section with the same formula as was used in Section III to convert ΔT_N to ASD.

V. Conclusion

Table 3 summarizes and compares the 100-s and, where available, the 10-s and 1000-s ASDs of the atmosphere and of the various retrieval errors discussed in this article. ASDs are given for high elevation angles (>60 deg) and low (20-deg) elevation angles. Cassini Gravity Wave Experiment requirements (which don't specify elevation angle) are given in the first row of Table 3; these are followed with the ASD of an uncalibrated atmosphere based on models used by Linfield [2], WVR measurements reported by Keihm [5], and the August 2001 AWVR measurements of Table 2. The greater-than symbols (>) in the 20-deg elevation column indicate that the ASD measurements are from the line-of-sight Cassini observations of Table 2 and that the ASDs for a fixed 20-deg elevation would be higher than indicated. The "worst," "best," and "typical" single-frequency 32-GHz retrieval ASDs from Table 2 are summarized next in Table 3. Again, the ">" symbol in the 20-deg elevation column indicates that the errors were computed from the line-of-sight path delay during Cassini tracks. Instrument and side-lobe errors follow, and in this case the less-than symbol (<) is used to indicate that the side-lobe errors were below the measurement noise floor.

The rss of retrieval and instrumental errors provides the final estimate of the path-delay performance one may expect from the 32-GHz embedded system. High/low estimates are provided based on the worst-/best-case retrieval and side-lobe errors. As can be seen in Table 3, at the 100-s time scales, the performance of the path-delay estimate is marginal: on some days the system would reduce the

Table 3. Summary results.

Requirement/model	ASD $\times 10^{-15}$ s/s					
	60- to 90-deg elevation			20-deg elevation		
	10 s	100 s	1000 s	10 s	100 s	1000 s
Cassini requirements	—	4.5	1.6	—	4.5	1.6
Atmosphere—Linfield'93	64	43	16	83	63	35
Atmosphere—Keihm'95 December average	—	11	5	—	—	—
Atmosphere—Keihm'95 July average	—	16	9	—	—	—
Atmosphere—high 08/21/01	—	37	—	—	>51.6	—
Atmosphere—low 08/25/01	—	9.2	—	—	>12.9	—
Atmosphere—typical 08/23/01	—	21.4	—	—	>33.5	—
Retrieval—worst 31 GHz 08/21/01	—	6.6	—	—	>7.4	—
Retrieval—best 31 GHz 08/22/01	—	1.0	—	—	>3.3	—
Retrieval—typical 08/23/01	—	2.3	—	—	>3.8	—
Amplifier stability (31 GHz; 1.3 cm/K)	—	8.7	1.7	—	13.1	2.6
$T_{sys}/\sqrt{BT}$ ($TBz = 10$ K at 31 GHz; 1.3 cm/K)	—	1.0	0.1	—	1.5	0.2
BWG side lobes (31 GHz; 1.3 cm/K)	—	<7.5	<0.8	—	22.5	2.3
RSS instrument and retrieval maximum	—	13.3	—	—	27.1	—
RSS instrument and retrieval minimum	—	8.8	—	—	26.3	—

atmospheric variability by a factor of two or three, and some days the performance would be worse than the uncalibrated atmosphere. In no case would the system meet Cassini requirements. Therefore, the system would be limited to use as a diagnostic tool and, possibly, as a means of limiting path-delay errors on bad days.

The results of Table 3 indicate a need for a dedicated Dicke radiometer with observation bands near 22 GHz. The sensitivity to water vapor is about three times higher at 22 GHz, which would reduce the relative sensitivity to side-lobe errors, and a chopped reference provided by the Dicke switch would stabilize the amplifier gain. The feasibility of embedding such a system in the beam-waveguide optics is beyond the scope of this article, but one can anticipate that the engineering problems will be significant since 22 GHz falls between the X- and Ka-band receivers, which are presently split by dichroic reflectors. The costs of such a system may be difficult to justify on the basis of meeting the path-delay performance on only the short time scales—especially if the communication-channel noise performance is compromised. A non-interfering and independent system would be preferable. One promising option that has been examined would place a dedicated WVR on the back side of the beam waveguide's subreflector. Studies have shown that such a system would meet the short time-scale requirements of Cassini [6]. Such a system could also be precisely calibrated in an absolute sense and thereby provide a useful noise-temperature and path-delay reference on all time scales.

References

[1] S. J. Keihm and K. A. Marsh, "Advanced Algorithm and System Development for Cassini Radio Science Tropospheric Calibration," *The Telecommunications and Data Acquisition Progress Report 42-127, July–September 1996*, Jet Propulsion Laboratory, Pasadena, California, pp. 1–20, November 15, 1996.
http://tmo.jpl.nasa.gov/tmo/progress_report/42-127/127A.pdf

[2] R. P. Linfield and J. Z. Wilcox, "Radio Metric Errors Due to Mismatch and Offset Between a DSN Antenna Beam and the Beam of a Troposphere Calibration Instrument," *The Telecommunications and Data Acquisition Progress Report 42-114, April–June 1993*, Jet Propulsion Laboratory, Pasadena, California, pp. 1–13, August 15, 1993.
http://tmo.jpl.nasa.gov/tmo/progress_report/42-114/114A.pdf

[3] D. D. Morabito, "The Efficiency Characterization of the DSS-13 34-Meter Beam-Waveguide Antenna at Ka-Band (32.0 and 33.7 GHz) and X-Band (8.4 GHz)," *The Telecommunications and Data Acquisition Progress Report 42-125, January–March 1996*, pp. 1-20, May 15, 1996.
http://tmo.jpl.nasa.gov/tmo/progress_report/42-125/125D.pdf

[4] Tanner, A. B., "Embedding a Water Vapor Radiometer in a DSN Antenna: Experimental Results From DSS 13," *The Telecommunications and Mission Operations Progress Report 42-143, July–September 2000*, Jet Propulsion Laboratory, Pasadena, California, pp. 1–23, November 15, 2000.
http://tmo.jpl.nasa.gov/tmo/progress_report/42-143/143M.pdf

[5] S. J. Keihm, "Water Vapor Radiometer Measurements of the Tropospheric Delay Fluctuations at Goldstone Over a Full Year," *The Telecommunications and Data Acquisition Progress Report 42-122, April–June 1995*, Jet Propulsion Laboratory, Pasadena, California, pp. 1–11, August 15, 1995.
http://tmo.jpl.nasa.gov/tmo/progress_report/42-122/122J.pdf

[6] R. Linfield, "Mounting a Water Vapor Radiometer on a DSN Antenna Subreflector: Benefits for Radio Science and Millimeter-Wavelength VLBI," *The Telecommunications and Mission Operations Progress Report 42-145, January–March 2001*, Jet Propulsion Laboratory, Pasadena, California, pp. 1–13, May 15, 2001.
http://tmo.jpl.nasa.gov/tmo/progress_report/42-145/145M.pdf